Transition from squeezing to dripping in a microfluidic T–shaped junction

By M. De Menech[1], P. Garstecki[2], F. Jousse[3] and H. A. Stone[4]

[1]Max–Planck Institute for the Physics of Complex Systems, Nöthnitzer Str. 38, 01187 Dresden, Germany

[2]Institute of Physical Chemistry, Polish Academy of Sciences, Kasprzaka 44/52, 01-224 Warsaw, Poland

[3]Unilever Corporate Research, Colworth House, Sharnbrook, Bedfordshire MK44 1LQ England

[4]Division of Engineering and Applied Sciences, Harvard University, Cambridge, Massachusetts 02138

(Received ?? and in revised form ??)

We describe the results of a numerical investigation of the dynamics of breakup of streams of immiscible fluids in the confined geometry of a microfluidic T–junction. We identify *three* distinct regimes of formation of droplets: *squeezing, dripping and jetting*, providing a unifying picture of emulsification processes typical for microfluidic systems. The *squeezing* mechanism of breakup is particular to microfluidic systems, since the physical confinement of the fluids has pronounced effects on the interfacial dynamics. In this regime the breakup process is driven chiefly by the buildup of pressure upstream of an emerging droplet and both the dynamics of breakup and the scaling of the sizes of droplets are influenced only very weakly by the value of the capillary number. The *dripping* regime, while apparently homologous to the unbounded case, is also significantly influenced by the constrained geometry; these effects modify the scaling law for the size of the droplets derived from the balance of interfacial and viscous stresses. Finally, the *jetting* regime sets in only at very high flow rates, or with low surface tension i.e., higher values of the capillary number, similarly as in the unbounded case.

1. Introduction

Multiphase flows in small, often microfluidic, devices are finding many uses, in part because of the realization that individual drops can act as controlled chemical containers (e.g. reference one of the ismagilov papers and the recent nature overview we have in the references) and also because modern measurement methods offer new opportunities for sensing, detection, rheology, etc. One basic feature of these studies is the need to control the drop size under different flow conditions and for different geometries of the device. Understanding the flows is closely related to more classical studies of drop breakup and emulsification in sheared, unbounded fluid systems (Rallison 1984; Stone 1994). Nevertheless, as we shall discuss, the confinement that naturally accompanies flow in small devices has significant qualitative and quantitative effects of the drop dynamics and breakup (Garstecki *et al.* 2005*d*, 2006; Guillot & Colin 2005). Here we report fully three-dimensional numerical simulations to understand and characterize drop formation in one common geometric element, a T-junction, used in many recent multiphase flow investigations.

A microfluidic T–junction geometry was first introduced for the controlled formation

of water–in–oil dispersions by Thorsen *et al.* (2001). The authors made the reasonable suggestion that the dynamics of droplet formation is dominated by the balance of tangential shear stresses and surface tension as expected in unbounded shear flows, via an analogy to breakup processes in shear and extensional flows (Taylor 1934; Rallison 1984; Stone 1994). A detailed experimental study of the T–junction configuration (Garstecki *et al.* 2006) identified a different (*squeezing*) mechanism that is directly connected to the confined geometry in which the drop is formed (see also a related report by Guillot & Colin (2005)) . It was proposed that when the capillary number is sufficiently small, the dominant contribution to the dynamics of breakup arises from the buildup of pressure upstream of the emerging droplet Garstecki *et al.* (2005*d*, 2006). This model results in a scaling law for the size of the droplets that is independent of the value of the capillary number and includes only the ratio of the rates of flow of the two immiscible fluids.

In this paper we describe the results of three–dimensional numerical simulations that provide a unifying picture of the dynamics of formation of droplets in microfluidic T–junction geometries that includes both of the aforementioned types of breakup. We confirm the existence of the "rate–of–flow–controlled" or "squeezing" breakup mechanism at low values of the capillary number Ca, the ratio between the viscous and surface tension stresses (Ca will be defined more precisely below). We provide the details of the dynamics (e.g. the numerical simulations confirm the fluctuations of pressure upstream of the immiscible tip postulated by Garstecki *et al.* (2006)). We identify a critical value of Ca at which the system transits into a shear–dominated or dripping mechanism of droplet formation. Also, we indicate the differences in drop formation in confined and unbounded systems. Finally, similarly to breakup into an unbounded fluid, we observe a transition from dripping to jetting at high values of the capillary number.

Due to the small size of the microchannels (widths on the order of 10 to 100 μm) and typical flow rates (1 μL/s), flows in microfluidic systems are dominated by viscous effects. The laminar flow regime, together with the typically large values of the Peclet number (measuring the ratio of the convective to diffusive transport), allow for an extensive control both in space and time over the transport of chemical substances (Kenis *et al.* 1999; Stone *et al.* 2004). This control, in conjunction with the ease of fabrication of the microfluidic devices (Duffy *et al.* 1998; McDonald *et al.* 2000), is one of the main features driving the interest in microfluidic systems for engineering and research applications. At the fundamental level, from the point of view of fluid dynamics, the laminar channel flow of a single Newtonian phase is not particularly interesting, as it can be described by the linear Stokes equations of motion. This behaviour is to be contrasted with a wide class of phenomena that have been uncovered with the first experiments on two–phase flows in microfluidic systems (Thorsen *et al.* 2001; Ganán-Calvo & Gordillo 2001; Anna *et al.* 2003; Dreyfus *et al.* 2003). The existence of an interface and the influence of interfacial tension introduce strong non–linearities in the flow, which are responsible for the appearance of a range of novel effects, some of which are particular to microfluidic systems when the interfacial dynamics is strongly influenced by the confinement of the fluids by the walls of the channel (Garstecki *et al.* 2005*d*,*b*,*c*, 2006).

The interest in detailed understanding of the emulsification processes in microfluidic systems is additionally motivated by the wide range of research on applications of microfluidic multiphase flows (see Table 1). Most of the applications require precise control over the process of formation of droplets or bubbles (e.g. Basaran (2002)), and characterization or, preferably understanding, of the scaling laws that describe the volume of the bubbles or droplets formed in the devices as a function of the material (e.g. viscosities, interfacial tension) and flow parameters (e.g. pressures or rates–of–flow applied to the system).

Application	Reference
Chemical processing	
micromixing inside drops	Song *et al.* (2003)
drops and slugs as mixing elements	Gunther *et al.* (2004), Garstecki *et al.* (2005*a*)
high–throughput screening	Zheng *et al.* (2003), Zheng & Ismagilov (2005)
kinetic analyses	Song & Ismagilov (2003)
organic chemistry	Cygan *et al.* (2005)
Bioanalysis	
diagnostic assays	Sia *et al.* (2004)
handling and/or analysis of living cells	He *et al.* (2005)
molecular evolution	Cornish (2006)
Material Science	
anisotropic particles	Dendukuri *et al.* (2005), Xu *et al.* (2005), Jeong *et al.* (2004), Jeong *et al.* (2005), Nisisako *et al.* (2004)
microcapsules	Takeuchi *et al.* (2005)
colloidal shells	Subramaniam *et al.* (2005)

TABLE 1. Examples of applications of multiphase flow in microfluidic devices. The above references are representative and are not meant to imply priority or to be exhaustive.

Several methods of formation of both bubbles and droplets have already been described (see table 2). In our work we chose to explore the dynamics of breakup in a planar T–junction geometry. A number of experimental studies are available for a range of fluids and speeds of flow. Both rate–of–flow–controlled breakup, and shear–driven breakup mechanisms are reported. Our aim is to verify numerically the details of the squeezing mechanism of breakup (Garstecki *et al.* 2005*d*, 2006), and to provide a unified picture of the dynamics that would include also the shear–driven formation of droplets (Thorsen *et al.* 2001).

Before we present out results, we sketch the characteristics of the two main dynamical regimes. Qualitatively, the rate–of–flow–controlled breakup (Garstecki *et al.* 2005*d*, 2006) can be described as follows (see Figure 1): the tip of the stream of the immiscible fluid enters the main channel, and because interfacial stresses dominate the shear stresses, the tip blocks almost the entirety of the cross–section of the main channel (the shear stresses exerted on the tip by the continuous fluid are not strong enough to deform the tip significantly away from an area minimizing shape). As a result, the continuous fluid is confined to thin films between the tip of the other immiscible fluid and the walls of the device. Flow in these thin films is subject to an increased viscous resistance, which leads to a build–up of pressure upstream of the tip (Stone 2005). This pressure is larger than the pressure in the immiscible tip, and the continuous fluid displaces the interface or squeezes the neck of the inner fluid which leads to breakup and detachment of a droplet. Notably, within this regime the breakup *is not* driven by interfacial stresses, at least not until the very last stage; the speed at which the neck of the immiscible thread collapses is proportional to the rate of flow of the continuous fluid, and does not depend significantly on the value of the interfacial tension, or on the values of the viscosities of either of the two fluids (Garstecki *et al.* 2005*d*). Within this regime one can expect that the volume of the droplet will be a function of the ratio of the rates of flow of the two fluids, and will not depend strongly on the value of the capillary number (Garstecki *et al.* 2006). In

Subject	Reference
Planar geometries	
flow–focusing	Anna *et al.* (2003), Garstecki *et al.* (2004), Xu & Nakajima (2004), Cubaud & Ho (2004), Dreyfus *et al.* (2003), Ward *et al.* (2005)
cross–flow	Thorsen *et al.* (2001), Song & Ismagilov (2003), Tice *et al.* (2004), Okushima *et al.* (2004), Blackmore *et al.* (2001), Gerdts *et al.* (2004), Zheng *et al.* (2003), Dendukuri *et al.* (2005), Garstecki *et al.* (2006), Guillot & Colin (2005)
diverging flow T–junction	Link *et al.* (2004), Engl *et al.* (2005)
Axi–symmetric geometries	
	Ganán-Calvo & Gordillo (2001), Takeuchi *et al.* (2005), Jeong *et al.* (2004), Jeong *et al.* (2005), Utada *et al.* (2005)
Non planar geometries	
	Sugiura *et al.* (2005), Sugiura *et al.* (2001)

TABLE 2. Examples of droplet and bubble formation in microfluidic devices. The above references are representative and are not meant to imply priority or to be exhaustive.

the shear–driven breakup, the volume of the droplet can be estimated from a balance of the viscous drag that the continuous fluid exerts on the emerging droplet and the interfacial force that opposes the elongation of the neck, which connects the reservoir of the discontinuous fluid with the droplet (e.g. Umbanhovar *et al.* (2000)). This model leads to a relation in which the diameter of the droplet is inversely proportional to the capillary number calculated for the flow of the continuous liquid. Because the drag force exerted on the droplet depends only very weakly on the viscosity of the droplet, within the shear-driven regime, the viscosity of the discontinuous phase does not influence the size of droplets appreciably (e.g. see discussion of flow past a drop in Batchelor (2000)). This effect has been confirmed experimentally by Cramer *et al.* (2004).

The qualitatively different predictions of each of the two models of breakup make it possible to distinguish between them by inspecting how the volume of the droplets depends on the material (viscosities and interfacial tension) and flow (rates of flow) parameters. An advantage of numerical simulations over the experiments is the control over the different parameters. In the experiments, for example, it is difficult to change the interfacial tension between the two fluids over a wide range of values without introducing dynamic surface tension effects (at low concentrations of surfactant), or changing the wetting properties of the two fluids. In contrast, in simulations it is straightforward to change the value of any parameter without affecting any others. Here we present the results of three–dimensional simulations for a range of the values of Ca that is broad enough to observe all three mechanisms of break-up in the confined geometry of a T-junction: squeezing, dripping and jetting.

We use a phase–field model (De Menech 2006) to describe the flow of the two fluids in the T–junction. The large interfacial tensions associated with the low capillary number characteristic of microfluidic flow can be handled due to the diffuse nature of the phase boundary separating the two fluids. The equilibrium properties of the mixture, including phase behaviour, wetting properties and the concentration profile in the interface region,

[htb]

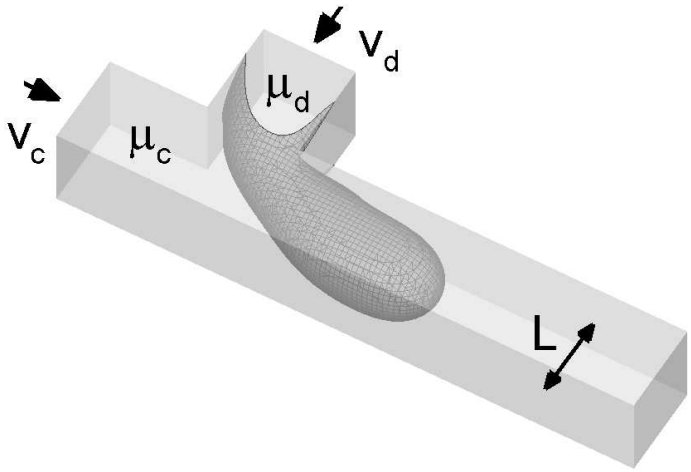

FIGURE 1. Diagram of a T–junction with cross flow. The channels have square cross section with side L. v_c and v_d are the mean flow velocities of the continuous and dispersed phases, while μ_c and μ_d are the corresponding shear viscosities.

are derived from a generalized free–energy functional, which determines also the diffusive and capillary forces in the transport equations. The transport equations are solved on a three–dimensional grid, and the method has been tested successfully in the case of droplet breakup in a T–junction with diverging flow (De Menech 2006).

In the following section we define the geometry and the parameters of the system that we study and introduce the important dimensionless quantities. In section 3 we describe the numerical methods employed in our work. In section 4 we detail the results, both for the low and high capillary number regimes, and we summarize our observations in section 5.

2. Description of the system

For a planar geometry, the characteristic dimensions of the T-shaped junction are the height h, and the widths of the main and side channels. We will consider the simplest case, in which the widths of both ducts equal L, and the channels have a square cross–section $h = L$ (figure 1). The dispersed phase is injected into the main channel from the side inlet. For simplicity, we set the densities of both phases equal; we expect that this choice has negligible influence on the results, as we investigate flows at the limit of vanishing Reynolds number. Besides the width L, which is constant, the problem is fully described by six parameters characterizing the flow and material properties of the fluids. These parameters are: the mean superficial speeds of the continuous and dispersed phases, v_c and v_d respectively, the viscosities of the two fluids μ_c and μ_d, the surface tension γ, and the density ρ. We will assume perfect wetting for the continuous phase, and the equilibrium contact angle for the dispersed fluid is set to 180°. The rescaled volume V/L^3 of the droplets formed in the device is the seventh physical quantity, and following the Buckingham-Π theorem, it can be described as a function of four

dimensionless parameters. We chose the following groups: the capillary number calculated for the continuous phase, $\mathrm{Ca} = \mu_c v_c/\gamma$, the Reynolds number $\mathrm{Re} = \rho v_c L/\mu_c$, the viscosity ratio $\lambda = \mu_d/\mu_c$, and the flow rate ratio $Q = v_d/v_c = Q_d/Q_c$, where $Q_d = v_d L^2$ and $Q_c = v_c L^2$ are the flow rates at the two inlets. The pressure will be rescaled by the viscous energy density $\mu_c v_c/L$, while the time unit is v_c/L.

For the flow regimes under consideration, the Reynolds number is small ($\mathrm{Re} < 1$), and does not influence the droplet size, which leaves us with the three governing parameters: Ca, λ, and Q. Our main focus is the discussion of the transition from the surface–tension dominated to the shear–dominated regime, which is best characterized by considering the effects of the capillary number on the droplet size. Within this framework, will also consider the influence of λ and Q.

3. Numerical method

The two–phase flow in the microfluidic device is described with a phase–field model (De Menech 2006), which includes the advection–diffusion equation for the molar fraction of one component and the Navier-Stokes equation with a Korteweg stress tensor, which is responsible for the development of surface stresses due to the presence of fluid–fluid and fluid–solid interfaces. The reactive and dissipative terms in the transport equations are derived from a generalized free–energy functional, which determines the equilibrium properties of the system, such as phase behavior and static wetting angles. The capillary stresses at the interfaces are represented as volume forces, and are distributed over the characteristic thickness ξ of the diffuse phase boundary. This important feature of the model allows the treatment of multiphase flows with relatively coarse grids, since typically only a few mesh points are needed to resolve the smooth variation of the order parameter across the interface. The interface thickness should be compared to a characteristic length of the system, which could be the radius of a droplet or the size of the domain (here L) in the case of constrained flow, leading to the definition of the Cahn number $\mathrm{C} = \xi/L$. The droplet dynamics of two immiscible fluids, described classically in the sharp interface limit $\xi \to 0$, is exactly recovered as C and the diffusivity go to zero (Jacqmin 1999). There are two possible ways to interpret the results of the phase–field model. The first one is to relate ξ to the physical width of the interface for real fluids, which is of the order of 1 nm. In this approach, our simulations should, within the continuum model, reflect the actual flow of fluids at the nano–scale, with typical channel width of the order of 10 nm.

Another interpretation is to consider the diffuse interface model as an approximation of the flow of immiscible fluids at the microscale, which is justified when the interface thickness ξ is small compared with the characteristic length of the flow L. Despite the fact that ξ is not the interface thickness separating real bulk fluids (e.g. since we typically choose $\mathrm{C} = 1/20$ for numerical convenience, then $\xi \sim 5\mu$m when simulating drops in 100 μm channels), the experimentally observed droplet dynamics in microfluidic devices can be effectively reproduced (De Menech 2006). The results that we describe in this report, which are expressed in terms of the non–dimensional groups, also match closely the experimental observation of flow of bubble formation in microfluidic T–junctions (Garstecki *et al.* 2006).

4. Results

As the dispersed phase enters from the side inlet into the main channel, it is distorted by the stresses exerted by the flow of the outer fluid, which acts to squeeze and stretch

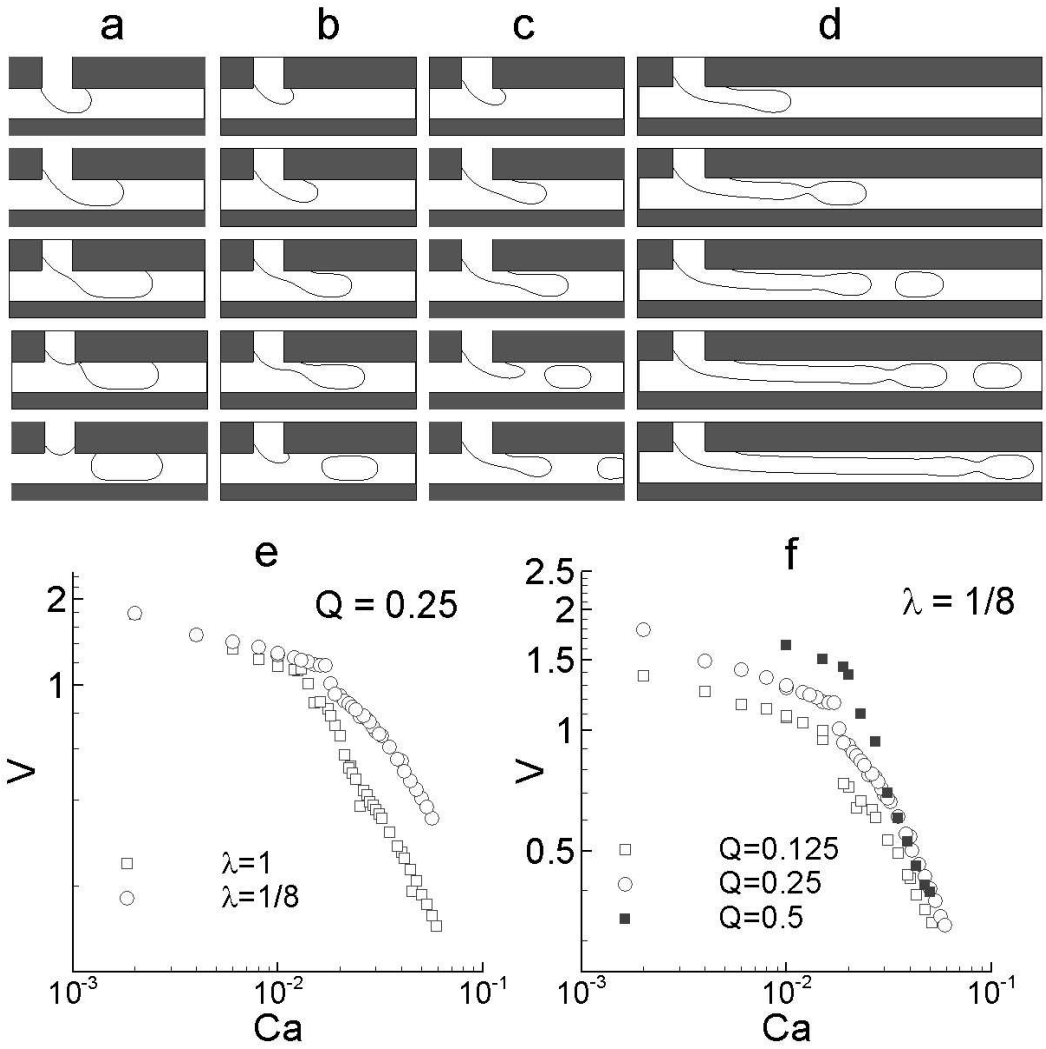

FIGURE 2. Drop formation as a function of capillary number. Top panels: two regimes of droplet formation are clearly distinguishable, at low (panel a, Ca = 0.002) and high (panels b and c, Ca = 0.035) Ca respectively. The onset of a jet at high Ca is illustrated in panel d (Ca = 0.05). Bottom figures: log–log plot of droplet volume versus capillary number. Panel e: $Q = 1/4$, and $\lambda = 1,\ 1/8$. Panel f: $\lambda = 1/8$, $Q = 1/8,\ 1/4$ and $1/2$. At high Ca the droplet volume decreases more steeply, and is strongly influenced by the viscosity ratio λ.

the inner fluid in the downstream direction (see Figure 1). Surface tension tends to resist this external force pulling the thread upstream and the dynamics of droplet formation in the channel will depend on the relative strengths of viscous and surface stresses. After an initial time transient, whose duration in time grows linearly with the capillary number and during which drops form aperiodically, we observe the regular formation of monodisperse droplets.

In Figure 2 we show a squence of images illustrating drop formation and report the measured droplet volume as a function of Ca in two different scenarios: allowing the viscosity ratio to change, while keeping Q fixed, or, conversely, varying Q while fixing

λ. We can clearly identify two different regions in both diagrams, at low and high Ca respectively. For a range of low Ca the droplet size does not change significantly, while beyond the critical value $\mathrm{Ca_c} \approx 0.015$, which is not a strong function of viscosity ratio, the droplet size decreases rapidly with the capillary number. Also, changing the viscosity contrast has little or no effect at low Ca, while it modifies quite sensibly the droplet volume at high Ca. The visualization of the droplet formation process (Figures 2a–c) shows that the two regimes of drop formation have qualitatively different characteristics. At low Ca the incoming thread tends to occupy the full width of the main channel, with the breakup occurring right at the junction (Figure 2a). At high Ca the dispersed fluid occupies only part of the main channel, and smaller droplets are formed downstream of the T-junction (Figures 2b–d), with dynamics that resembles more and more that of the classical pendant–drop problem in a coflow geometry (Umbanhovar *et al.* 2000; Cramer *et al.* 2004). We will in fact show that this dripping regime has significant differences from the unbound coflow case, since even for high Ca the droplets occupy a significant portion of the main channel, which in turn affects the flow field of the outer continuous–phase fluid. In addition, we report in the panel of Figure 2d some snapshots of the development of the thread for a high capillary number: the droplet detachment point gradually moves downstream, until a stable jet is formed, whose length is limited by the size of the simulation domain.

4.1. *Low* Ca*: the squeezing regime*

Numerical simulations allow access to all of the dynamical variables of the system. For example, we can monitor the evolution of the droplet formation by looking at the time dependence of the pressure in the continuous fluid immediately upstream of the tip of the discontinuous phase. This evolution of pressure at the junction lies at the heart of the interfacial dynamics in the squeezing regime (Garstecki *et al.* 2005*d*, 2006). Qualitatively, at low values of Ca, the tip of the discontinuous fluid effectively blocks almost the entirety of the cross–section of the main duct, and obstructs the flow of the continuous fluid. Regardless of the type of forcing, either fixed rate of flow or fixed pressure at the inlet of the continuous fluid, the obstruction of the main channel leads to an increase of pressure upstream of the tip of the discontinuous fluid. We observe the details of the evolution of pressure in our numerical simulations.

As the discontinuous–phase fluid enters the junction the pressure rises gradually until the channel is blocked (steps a–b in Figure 3); this time interval is defined as the blocking time, τ_{block}. At this stage the continuous flow begins to squeeze the neck of the thread (steps b–c), until breakup occurs, and the pressure drops abruptly (steps c–d). The time interval from steps (b) to (d) is defined as squeezing time, τ_{squeeze}. The viscosity contrast determines the details of the pressure profile in the squeezing phase, while its duration remains unaffected.

Also, we considered the behaviour of the pressure profile upstream of the junction for fixed Q and λ, while varying the capillary number, $\mathrm{Ca} \ll 1$ (Figure 4). We observe that τ_{squeeze} is independent of Ca, while the blocking time grows as Ca is decreased. The results in Figures 3 and 4 therefore confirm the intuitive fact that τ_{squeeze} depends only on the velocity of the outer fluid, which is responsible for the buildup of the pressure that is required to compress the neck, whose displacement will progress at a rate proportional to the flux of the dispersed phase.

When $Q_d \gg Q_c$ we expect $\tau_{\mathrm{squeeze}} \gg \tau_{\mathrm{block}}$ and the total time for droplet formation $\tau = \tau_{\mathrm{block}} + \tau_{\mathrm{squeeze}}$ depends only on τ_{squeeze}, which suggests the relation $\tau \propto 1/Q_c$. The volume of the droplet will therefore be $V_d = \tau Q_d \propto Q$. On the other hand, if $Q_d \ll Q_c$, $\tau \approx \tau_{\mathrm{block}}$ depends on the distance the breakup point has to travel from the side inlet to

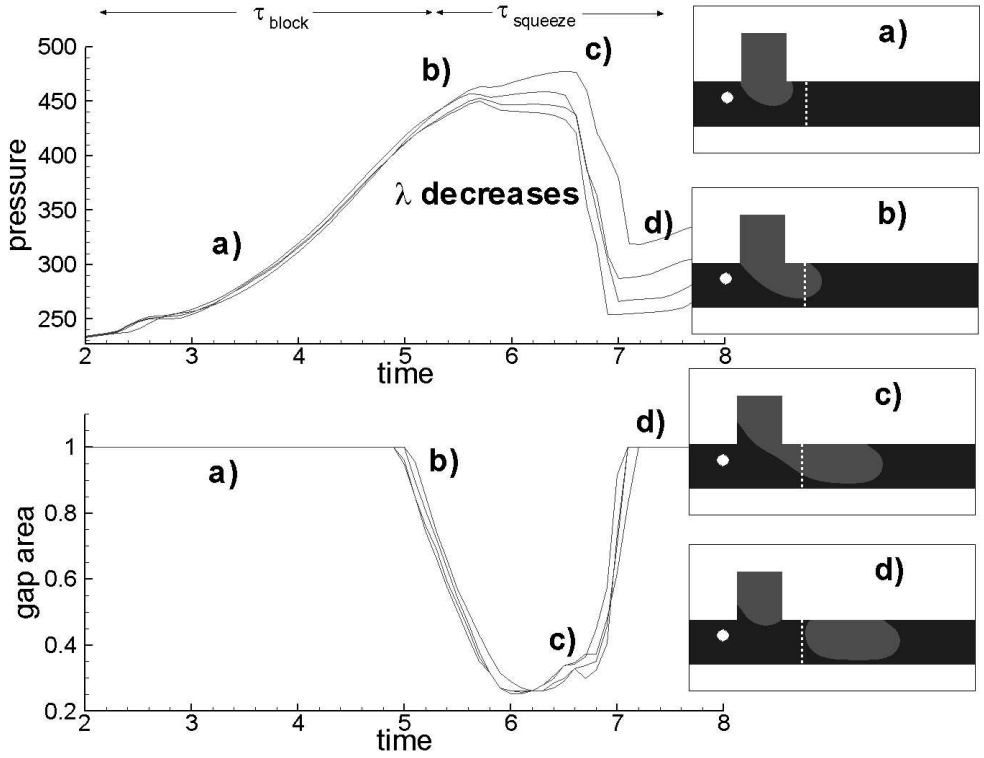

FIGURE 3. Pressure upstream of the T–junction (top) and area of the gap between the dispersed phase and the channel walls downstream (bottom) as a function of time; Ca = 0.01. The frames on the right visualize different stages of the droplet formation process. The pressure was measured at the position marked by the white dot, while the gap area is taken over a plane marked by the dashed line. We identify the two main steps of droplet formation: the interval (a)–(b) mark the blocking phase, while from (b) to (d) the thread is squeezed until breakup occurs. Four curves are shown for each plot, with $\lambda = 1, 1/2, 1/4$ and $1/8$. The pressure profile in the squeezing phase varies, somewhat weakly, with the viscosity ratio: as λ decreases the pressure profile becomes smoother in the interval from the end of the blocking stage (b) to the breakup point (d).

enter the junction and on the flow rate Q_d. Thus, we expect $\tau = \tau_{\text{block}} \propto 1/Q_d$, which implies $V_d = \tau Q_d \propto$ constant that is independent of the flow ratio Q. The two regimes can be combined in the simple dimensionless relation $V \propto 1 + \alpha Q$, where $V = V_d/L^3$ is the scaled drop volume and α is a constant which may depend on the widths of the two channels. This mechanism was first proposed by Garstecki et al. (Garstecki *et al.* 2006), where the functional form $V(Q)$ was observed experimentally. Cubaud *et al.* (2005) observed a similar behaviour for bubble formation in a symmetric cross junction. We verified this result with our numerical simulations. Figure 5 shows the variation of the volume with Q for three values of λ; the data collapse over the same straight line $V = 1 + 2Q$.

4.2. *Transition from low to high* Ca

As we increase the capillary number, while keeping the flow rates unchanged, we move away from the squeezing regime described in the previous section; in particular we observe that the drop volume (Figure 2) drops sharply with Ca, and there is a strong dependence on the viscosity ratio. One observes that the incoming fluid blocks only partially the main

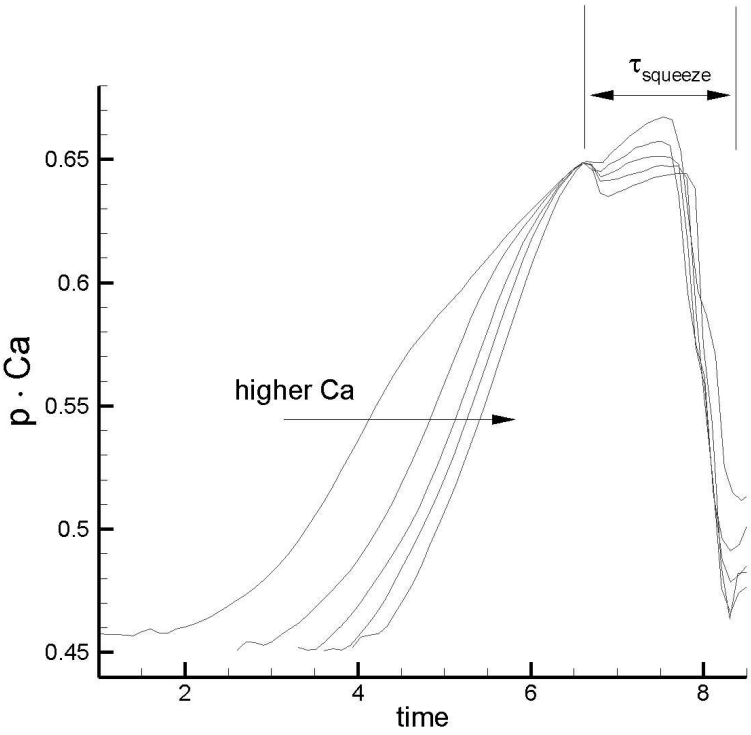

FIGURE 4. Time variation of the upstream pressure profile, scaled by the capillary number (Ca $= 0.002, 0.004, 0.006, 0.008$ and 0.01 following the arrow from left to right). The time to achieve blocking decreases as the surface tension is decreased, while the squeezing time remains unchanged. $\lambda = 1$ and $Q = 1/4$.

channel (Figures 2b–c), and that the breakup point moves downstream of the T–junction. This last effect is much more marked for $\lambda = 1$. The overall trends are consistent with that observed for unbounded coflow, where the breakup point moves away from the inlet for higher viscosities of the dispersed phase (Zhang & Stone 1997; Cramer *et al.* 2004). On the other hand, in the unbounded case the droplet size is approximately independent of the viscosity ratio, which is in clear contrast with the results of our simulations. The explanation for such marked difference is related to the constrained geometry: here, due to the presence of the droplet, the changes in the flow of the outer fluid cannot be neglected.

We next contrast directly the pressure fluctuations, which accompany droplet formation, for the sequeezing regime (Ca $\lesssim 0.01$) and dripping regime (Ca $\gtrsim 0.02$); detailed results are given in Figures 6 and 7. We observe that for $\lambda = 1$ the pressure fluctuations upstream of the T–junction decrease drastically as we move from the squeezing to the dripping regime. The perturbation of the outer flow due to the presence of the droplet in the channel is drastically reduced, and the main driving force for the necking of the thread is the shear force. On the other hand, pressure fluctuations maintain a much larger amplitude for $\lambda = 1/8$: droplet formation is still governed by the squeezing mechanism, while there might be some effect due to shear. Similar to the volume versus Ca plot of Figure 2, we demonstrate the different qualitative nature of the squeezing and dripping regimes by considering the variation of the pressure fluctuations Δp (Figure 7). While for low Ca the amplitude remains constant, in the dripping regime there is a clear decrease,

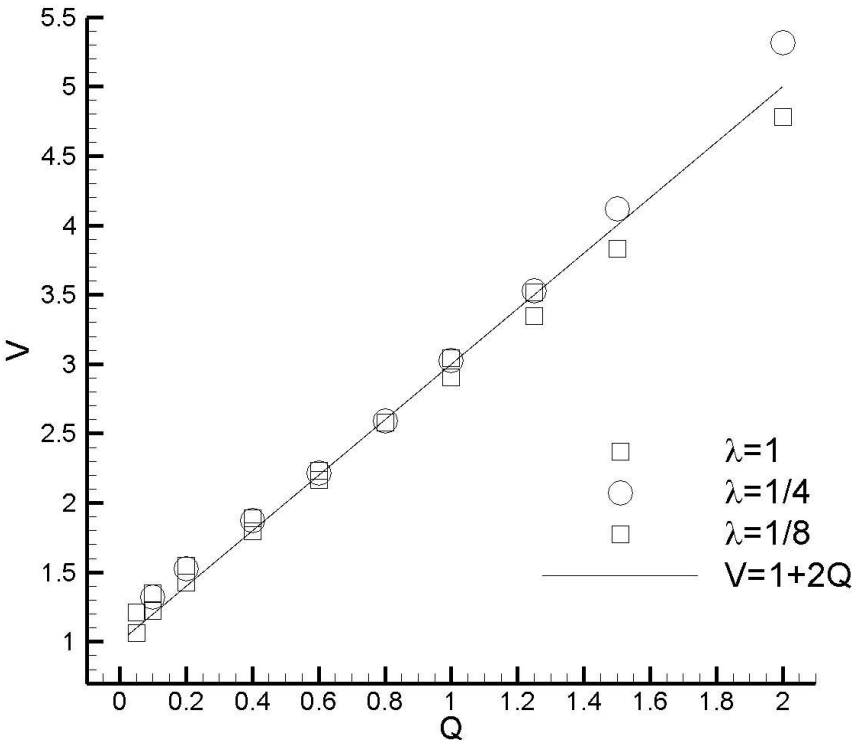

FIGURE 5. Variation of the dimensionless droplet volume with flow rate ratio for low capillary number, Ca = 0.005.

which is well pronounced for $\lambda = 1$, and more gradual for $\lambda = 1/8$. We believe that this behaviour – of a more gradual transition to dripping at lower values of λ – suggests that the description of the dynamics of breakup with the use of the capillary number calculated only for the continuous phase is not sufficient. For λ significantly different than unity, one should take into account an effective capillary number calculated on the basis of capillary numbers for both phases.

4.3. *High* Ca*: the dripping regime*

In order to clarify the role of shear stresses in the dripping regime, we consider two model scaling relations proposed by Umbanhovar *et al.* (2000) for breakup in a coflowing unbounded fluid, and by Thorsen *et al.* (2001) for breakup in a T–junction. In both cases one assumes that breakup occurs when the interfacial force is nearly balanced by the shear force, such that $r \sim \sigma/(\mu\,\dot{\varepsilon})$ where r is the final droplet radius and $\dot{\varepsilon}$ is the shear rate exerted on the droplet, based upon the mean speed of flow of the continuous phase. Thorsen *et al.* (2001) took into account the fact that the emerging droplet decreases the cross–section of the channel available for the flow of the continuous fluid. In order to maintain the volumetric rate of flow, the continuous phase flows faster through the gap between the droplet and the wall of the channel, compared to the case of an unobstructed channel, and exerts a larger shear stress on the droplet. This effect, in turn, results in smaller size of the droplets that are formed in confined geometry – smaller than for the

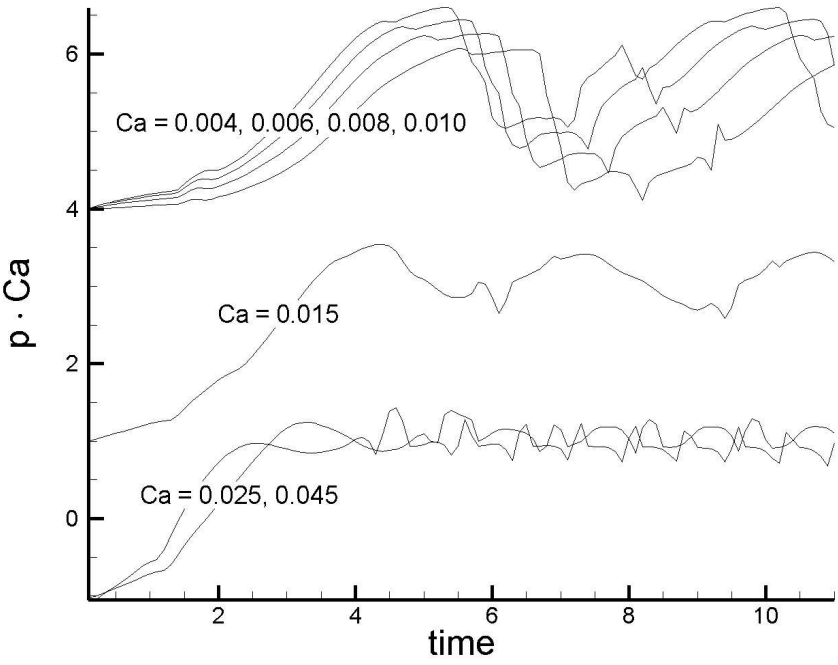

FIGURE 6. Pressure as a function of time upstream of the T–junction for different values of the capillary number. The oscillations correspond to the droplet formation frequency; as Ca is increased, the frequency increases while the amplitude of the pressure fluctuations drops, as shown in the curves from top to bottom. The pressure on the vertical axis is rescaled by the capillary number, such that the amplitude of the fluctuations can be reported on the same scale for both the squeezing regime (Ca < 0.015) and the dripping regime (Ca > 0.015). $\lambda = 1$ and $Q = 1/4$.

same superficial speed of flow of the continuous fluid in an unbounded case. In particular Thorsen *et al.* (2001) calculated the shear stress on the basis of the measured size of the gap between the dispersed fluid and the side walls of the main channel. We performed a similar analysis: we measured the gap area in our simulations, and estimated $\dot{\varepsilon}$ as the ratio between the average flow speed in the gap, v_g, and linear width of the gap, L_g, estimated by the square root of the cross section of the gap. We will use the rescaled shear rate $\dot{\varepsilon}_{\rm d} = \dot{\varepsilon} L / v_d$. Based on the dimensionless groups, we write

$$R = \frac{r}{L} \sim \frac{1}{\mathrm{Ca}\, \dot{\varepsilon}_{\rm d}}. \tag{4.1}$$

In Figure 8 we plot the radius of the droplet calculated on the basis of equation (4.1) and compare it to the radius measured in our simulations. The prediction overshoots by an order of magnitude the actual radius. In fact, in (Thorsen *et al.* 2001) the calculated radii of the droplets were also systematically larger than the observed values. This discrepancy is in fact consistent with the general observation that droplet breakup is much easier in microfluidic devices than for unbounded flows. Even considering the actual shear flow in the breakup region, the critical capillary number can easily be ten times smaller than for free flow conditions (Link *et al.* 2004). From our simulations of the dripping regime

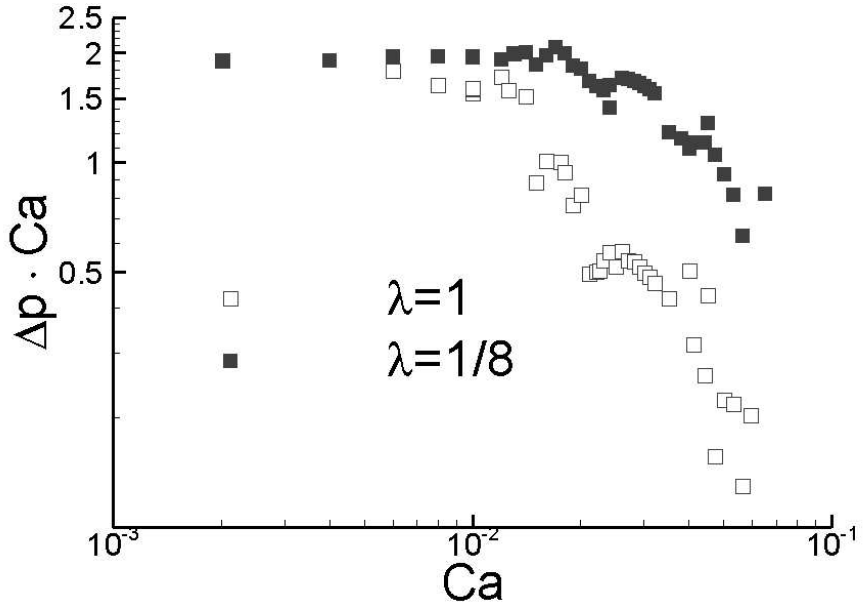

FIGURE 7. Variation of the pressure fluctuation Δp upstream the T–junction with the capillary number for two values of the viscosity ratio, $\lambda = 1$ and $\lambda = 1/8$. The pressure is rescaled by the surface tension by multiplying by the capillary number Ca. Similar to Figure 2, this diagram clearly illustrates the transition from the squeezing regime to the dripping regime, where there is a strong dependence on the viscosity ratio.

we find $R \sim 1/(\mathrm{Ca}\ \dot{\varepsilon}_\mathrm{d})^{0.4}$, i.e. the radius of the droplet increases far more slowly than one would expect form the scaling law (4.1). All the observations above point to the fact that there are additional forces exerted on the droplet that pull it downstream and speed up the breakup. Observing that even in the dripping regime the droplets typically occupy a substantial portion of the cross–section of the microchannel, we can associate this additional force with an elevated pressure drop along the length of the emerging droplet (Stone 2005), which is the same effect that played the dominant role in the squeezing regime.

Summarizing, although the process of formation of droplets in the dripping regime is reminiscent of dripping in coflow in an unbounded fluid, it is fundamentally different because the pressure effects are never negligible, unless the radius of the droplet is much smaller than the width of the channel. Combination of shear stresses and the pressure makes quantitative analysis of the scaling of the size of the droplets formed in this regime particularly difficult (note that the range of the values of capillary number over which we observe dripping is quite small). As the capillary number is further increased the breakup point moves progressively downstream from cycle to cycle, and a jet is formed. There clearly is a transition from the stable dripping regime to a jetting regime. We were not, however, able to explore this regime in detail, as it requires very large simulation boxes.

5. Discussion

Our numerical study of the dynamics of breakup in a T–junction has revealed three distinct regimes of formation of droplets: squeezing, dripping and jetting. The first regime – squeezing – is particular to microfluidic geometries because it depends crucially on

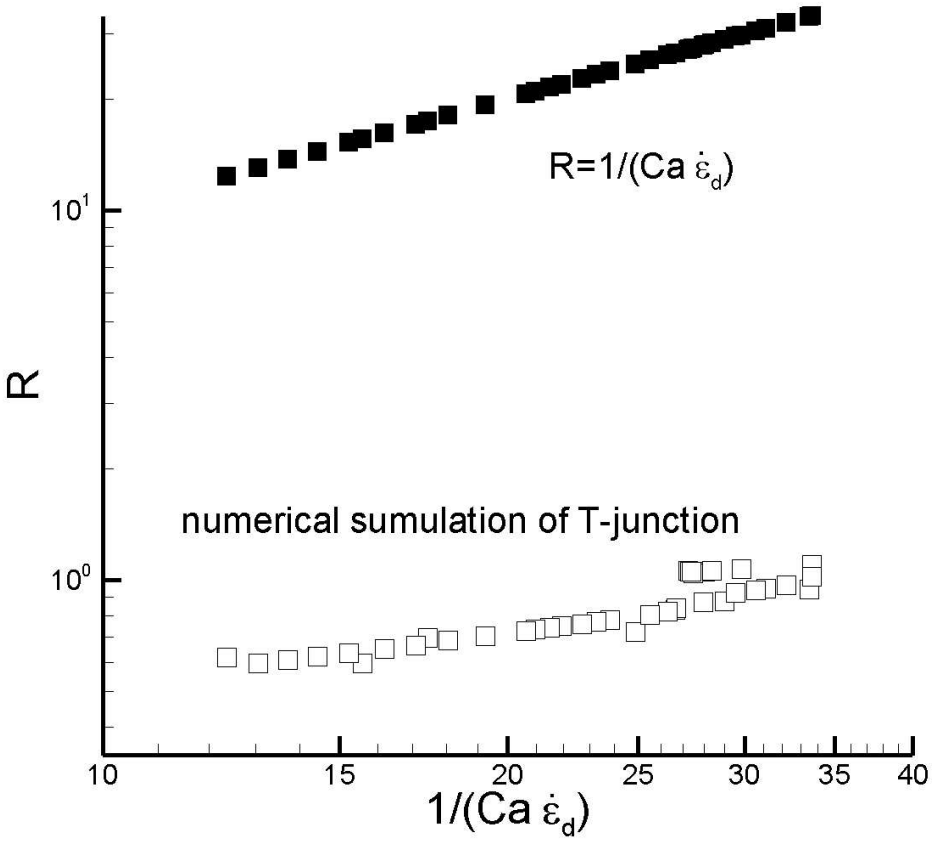

FIGURE 8. Variation of the droplet radius with the ratio between surface tension stresses and shear stresses, equal to $1/(\mathrm{Ca}\ \dot{\varepsilon}_\mathrm{d})$, where Ca is the capillary number and $\dot{\varepsilon}_\mathrm{d}$ is the dimensionless shear rate of the continuous phase. The data refer to the dripping regime ($\mathrm{Ca} > 0.015$). $Q = 1/4$, $\lambda = 1$.

strong physical confinement of the interfacial dynamics. The evolution of pressure that we observe in our simulations upstream of the emerging droplet confirms the model of break-up proposed in Garstecki *et al.* (2006) and Guillot & Colin (2005). In this regime the dominating contribution in the dynamics of break-up arises from the buildup of pressure, which results from the blocking of the cross-section of the main channel by the tip of the discontinuous phase. We observe this regime at low values of capillary numbers with the transition to a regime in which the shear stresses exerted on the emerging droplet begin to play a significant role at $\mathrm{Ca} \sim 0.015$ for $\lambda = 1$, and at slightly higher values for $\lambda = 1/8$. The size (volume) of the droplets and bubbles formed in the squeezing regime can be described by a simple scaling relation of the form: $V = 1 + \alpha Q$, where α is a constant of order unity, who's exact value depends on the geometry of the T-junction, and is independent of λ Garstecki *et al.* (2006). There are two important characteristics of the squeezing regime: i) the lack of dependence of the size of the droplets (bubbles) on material parameters (e.g. viscosities of the fluids, or interfacial tension) make this mode

of break-up particularly simple for use in applications, allowing for varying the fluids without altering the dynamics of formation of the discrete elements of fluid, and ii) the fact that break-up in this regime is not driven by shear stresses exerted on the emerging droplets (bubbles) allows for emulsification in conditions in which the capillary number can be very small – that is even in very small devices and at very small rates of flow.

We observe that the dripping, or shear–driven, breakup regime, is strongly modified in the microfluidic setting of a T-junction geometry with respect to the analogous mode of break-up in unbounded fluids, due to the effects of confinement. Even when the shear stresses exerted on the emerging droplet are able to deform it substantially, it still occupies a significant portion of the cross-section of the channel. Thus, the effects of buildup of pressure upstream of the emerging droplet are still present, and they modify the condition for break-up (facilitating it). Due to a small range of the values of the capillary number over which we observe dripping – before it is replaced by jetting – is is not reasonable to propose any scaling relation for the size of the droplets formed in this regime. In the jetting regime the stream of the discontinuous fluid extends downstream of the T-junction and the two immiscible fluids flow laminarly side-by-side over lengths of the channel which are several times larger than its width.

6. Acknowledgements

MDM acknowledges support from Unilever Corporate Research and the European Union (MRTN-CT-2004-005728). HAS thanks the Harvard MRSEC (DMR–0213805) for partial support. PG thanks the Foundation for Polish Science for financial support.

REFERENCES

Anna, S., Bontoux, N. & Stone, H. A. 2003 Formation of dispersions using flow focusing in microchannels. *Appl. Phys. Lett.* **82**, 364–366.

Basaran, O. A. 2002 Small-scale free surface flows with breakup: Dropo formation and emerging applications. *AIChE* **48**, 1842–1848.

Batchelor, G. K. 2000 *An Introduction to Fluid Mechanics*. Cambridge University Press.

Blackmore, B., Li, D. Q. & Gao, J. 2001 Detachment of bubbles in slit microchannels by shearing flow. *J. Coll. Int. Sci.* **241**, 514–520.

Cornish, V. W. 2006 Catalytic competition for cells. *Nature* **440**, 156–157.

Cramer, C., Fischer, P. & Windhab, E. J. 2004 Drop formation in a co–flowing ambient fluid. *Chem Eng. Sci.* **59**, 3045–3058.

Cubaud, T. & Ho, C. M. 2004 Transport of bubbles in square microchannels. *Phys. Fluids* **16**, 4575–4585.

Cubaud, T., Tatieni, M. T., Zhong, X. & Ho, C. M. 2005 Bubble dispenser in microfluidic devices. *Phys. Rev. E* **172**, 037302.

Cygan, Z. T., Cabral, J. T., Beers, K. L. & Amis, E. J. 2005 Microfluidic platform for the generation of organic-phase microreactors. *Langmuir* **21**, 3629–3634.

De Menech, M. 2006 Modeling of droplet breakup in a microfluidic T–shaped junction. *Phys. Rev. E* **to appear**.

Dendukuri, D., Tsoi, K., Hatton, T. A. & Doyle, P. S. 2005 Controlled syntehsis of nonshperical microparticles using microfluidics. *Langmuir* **21**, 2113–2116.

Dreyfus, R., Tabeling, P. & Willaime, H. 2003 Ordered and disordered patterns in two-phase flows in microchannels. *Phys. Rev. Lett.* **90**, 144505.

Duffy, D. C., McDonald, J. C., Schueller, O. J. A. & Whitesides, G. M. 1998 Rapid prototyping of microfluidic systems in poly(dimetilsiloxane). *Ann. Chem.* **70**, 4974–4984.

Engl, W., Roche, M., Colin, A., Panizza, P. & Ajdari, A. 2005 Droplet traffic at a simple junction at low capillary numbers. *Phys. Rev. Lett.* **95**, 208305.

Ganán-Calvo, A. M. & Gordillo, J. M. 2001 Perfectly monodisperse microbubbling by capillary flow focusing. *Phys. Rev. Lett.* **87**, 274501.

Garstecki, P., Feuerstman, M., Stone, H. A. & Whitesides, G. M. 2006 Formation of droplets and bubbles in a microfluidic T–junction: scaling and mechanism of breakup. *Lab Chip* **6**, 437–446.

Garstecki, P., Fuerstman, M. & Whitesides, G. M. 2005*a* Desgin for mixing using bubbles in branched microfluidic channels. *Appl. Phys. Lett.* **86**, 244108.

Garstecki, P., Fuerstman, M. & Whitesides, G. M. 2005*b* Nonlinear dynamics of a microfluidic flow-focusing bubble generator. *Phys. Rev. Lett.* **94**, 234502.

Garstecki, P., Fuerstman, M. & Whitesides, G. M. 2005*c* Oscillations with uniquely long periods in a microfluidic bubble generator. *Nature Physics* **1**, 168–171.

Garstecki, P., Gitlin, I., DiLuzio, W., Whitesides, G., Kumacheva, E. & Stone, H. A. 2004 Formation of monodisperse bubbles in a microfluidic flow–focusing device. *Appl. Phys. Lett.* **85**, 2649–2651.

Garstecki, P., Stone, H. A. & Whitesides, G. M. 2005*d* Mechanisms for flow–rate controlled breakup in confined geometries: A route to monodisperse emulsions. *Phys. Rev. Lett.* **94**, 164501.

Gerdts, C. J., Sharoyan, D. E. & Ismagilov, R. F. 2004 A synthetic reaction network: Chemical amplification using nonequilibrium autocatalytic reactions coupled in time. *J. Am. Chem. Soc.* **126**, 6327–6331.

Guillot, P. & Colin, A. 2005 Stability of parallel flows in a microchannel after a T junction. *Phys. Rev. E* **72**, 066301.

Gunther, A., Kahn, S. A., Thalmann, M., Trachsel, F., Jensen, K. F. & Rallison, J. M. 2004 Transport and reaction in microscale segmented gas–liquid. *Lab Chip* **4**, 278–286.

He, M. Y., Edgar, J. S., Jeffries, G. D. M., R. M. Lorenz, J. P. S. & Chiu, D. T. 2005 Selective encapsulation of single cells and subcellular organelles into picoliter-and femtoliter-volume droplets. *Ann. Chem.* **77**, 1539–1544.

Jacqmin, D. 1999 Calculation of two–phase Navier–Stokes flows using phase–field modelling. *J. Comp. Phys.* **155**, 96–127.

Jeong, W., Kim, J. Y., Kim, S., Lee, S., Mensing, G. & Beebe, D. J. 2004 Hydrodynamic microfabrication via "on the fly" photopolymerization of microscale fibers and tubes. *Lab Chip* **4**, 576–580.

Jeong, W. J., Kim, J. Y., Choo, J., Lee, E. K., Han, C. S., Beebe, D. J., Seong, G. H. & Lee, S. H. 2005 Continuous fabrication of biocatalyst immobilized microparticles using photopolymerization and immiscible liquids in microfluidic systems. *Langmuir* **21**, 3738–3741.

Kenis, P. J. A., Ismagilov, R. F. & Whitesides, G. M. 1999 Microfabrication inside capillaries using multiphase laminar flow patterning. *Science* **285**, 83–85.

Link, D. R., Anna, S. L., Weitz, D. A. & Stone, H. A. 2004 Geometrically mediated breakup of drops in microfluidic devices. *Phys. Rev. Lett.* **92**, 053403.

McDonald, J. C., Duffy, D. C., Anderson, J. R., Chiu, D. T., Wu, H., Schueller, O. J. A. & Whitesides, G. M. 2000 Fabrication of microfluidic systems in poly(dimetilsiloxane). *Electrophoresis* **21–40**, 27.

Nisisako, T., Torii, T. & Higuchi, T. 2004 Novel microreactors for functional polymer beads. *Chem. Eng. J.* **101**, 23–29.

Okushima, S., Nisisako, T., Torii, T. & Higuchi, T. 2004 Controlled production of monodisperse double emulsions by two–step breakup in microfluidic devices. *Langmuir* **20**, 9905–9908.

Rallison, J. M. 1984 The deformation of small viscous drops and bubbles in viscous flow. *Ann. Rev. Fluid. Mech.* **16**, 45–66.

Sia, S. K., Linder, V., Parviz, B. A., Siegel, A. & Whitesides, G. M. 2004 An integrated approach to a portable low-cost immunoessay for resource-poor settings. *Angew. Chem., Int. Ed.* **43**, 498–502.

Song, H., Bringer, M. R., Tice, J. D., Gerdts, C. J. & Ismagilov, R. F. 2003 Experimental test of scaling of mixing by chaotic advection moving through microfluidic channels. *Appl. Phys. Lett.* **83**, 4664–4666.

Song, H. & Ismagilov, R. F. 2003 Millisecond kinetics on a microfluidic chip in multiphase microfluidics at low values of the Reynolds and capillary numbers. *J. Am. Chem. Soc.* **125**, 14613.

Stone, H. A. 1994 Dynamics of drop deformation and breakup in viscous fluids. *Ann. Rev. Fluid. Mech.* **26**, 65.

Stone, H. A. 2005 On lubrication flows in geometries with zero curvature. *Chem. Eng. Sci.* **60**, 4838.

Stone, H. A., Stroock, A. D. & Ajdari, A. 2004 Engineering flows in small devices: Microfluidics toward a lab-on-a-chip. *Ann. Rev. Fluid. Mech* **36**, 381–411.

Subramaniam, A. B., Abakarian, M. & Stone, H. A. 2005 Controlled assembly of jammed colloidal shells on fluid droplets. *Nature Materials* **4**, 553–556.

Sugiura, S., Nakajima, M., Iwamoto, S. & Seki, M. 2001 Interfacial tension driven monodisperse droplet formation form microfabricated channel array. *Langmuir* **17**, 5562–5566.

Sugiura, S., Oda, T., Izumida, Y., Aoyagi, Y., Satake, M., Ochiai, A. & Ohkohchi, N. 2005 Size control of calcium alginate beads containing living cells using micro-nozzle array. *Biomaterials* **26**, 3327–3331.

Takeuchi, S., Garstecki, P., Weibel, D. B. & Whitesides, G. M. 2005 An asxisymmetric flow–focusing microfluidic device. *Adv. Materials* **17**, 1067–1072.

Taylor, G. I. 1934 The formation of emulsions in definable fields of flow. *Proc. Roy. Soc. London A* **146**, 501–23.

Thorsen, T., Roberts, R. W., Arnold, F. H. & Quake, S. R. 2001 Dynamic pattern formation in a vesicle–generating microfluidic device. *Phys. Rev. Lett.* **86**, 4163–4166.

Tice, J. D., Lyon, A. D. & Ismagilov, R. F. 2004 Effects of viscosity on droplet formation and mixing in microlfuidic channels. *An. Chim. Acta* **507**, 73–77.

Umbanhovar, P. B., Prasad, V. & Weitz, D. A. 2000 Monodisperse emulsion generation via drop break off in a coflowing stream. *Langmuir* **16**, 347–351.

Utada, A. S., Lorenceau, E., Link, D. R., Kaplan, R. D., Stone, H. A. & Weitz, D. A. 2005 Monodisperse double emulsions generated from a microcapillary device. *Science* **308**, 537–541.

Ward, T., Faivre, M., .Abkarian, M. & Stone, H. A. 2005 Microfluidic flow focusing: Drop size and scaling in pressure versus flow–rate–driven pumping. *Electrophoresis* **26**, 3716–3724.

Xu, Q. & Nakajima, M. 2004 The generation of highly monodisperse droplets through the breakup of hydrodynamically focused microthread in a microfluidic device. *App. Phys. Lett.* **85**, 3726–3728.

Xu, S. Q., Nie, Z. H., Seo, M., Lewis, P., Kumacheva, E., Stone, H. A., Garstecki, P., Weibel, D. B., Gitlin, I. & Whitesides, G. M. 2005 Generation of monodisperse particles by using microlfuidics: control over size, shape, and composition. *Angew. Chem., Int. Ed.* **44**, 724–728.

Zhang, D. F. & Stone, H. A. 1997 Drop formation in viscous flows at a vertical capillary tube. *Phys. Fluids* **9**, 2234–2242.

Zheng, B. & Ismagilov, R. F. 2005 A microfluidic approach for screening submicroliter volumes against multiple reagents by using preformed arrays of nanoliter plugs in a three-phase liquid/liquid/gas flow. *Angew. Chem., Int. Ed. Engl.* **44**, 2520–2523.

Zheng, B., Roach, L. S. & Ismagilov, R. F. 2003 Screening of protein crystallization conditions on a microfluidic chip using nanoliter-size droplets. *J. Am. Chem. Soc.* **125**, 11170–11171.